Applied Physics Letters

Enhanced resistive memory in Nb-doped $BaTiO_3$ ferroelectric diodes

Cite as: Appl. Phys. Lett. **111**, 032902 (2017); https://doi.org/10.1063/1.4993938
Submitted: 25 April 2017 . Accepted: 01 July 2017 . Published Online: 17 July 2017

Qiao Jin, Chunyan Zheng, Yongcheng Zhang, Chaojing Lu, Jiyan Dai, and Zheng Wen

Enhanced resistive memory in Nb-doped $BaTiO_3$ ferroelectric diodes

Qiao Jin,[1] Chunyan Zheng,[1] Yongcheng Zhang,[1] Chaojing Lu,[1] Jiyan Dai,[2] and Zheng Wen[1,2,a)]
[1]College of Physics, Qingdao University, Qingdao 266071, China
[2]Department of Applied Physics, The Hong Kong Polytechnic University, Hong Kong 999077, China

(Received 25 April 2017; accepted 1 July 2017; published online 17 July 2017)

In this study, we report on enhanced resistive memory in $BaTiO_3$-based ferroelectric diodes due to the doping of donors. A large ON/OFF current ratio of ~2000, about two orders of magnitude higher than that of Au/$BaTiO_3$/$SrRuO_3$, is achieved in a Au/Nb:$BaTiO_3$/$SrRuO_3$ diode at room temperature. This can be ascribed to the enhanced ferroelectric-modulation on the potential barrier at the Nb:$BaTiO_3$/$SrRuO_3$ interface associated with the $(Nb_{Ti^{4+}}^{5+})^{\cdot}$ donors, which gives rise to an efficient control of device transport between a bulk-limited current in the ON state and an interface-limited Schottky emission in the OFF state. In contrast, the resistance switching is suppressed in a Au/Fe:$BaTiO_3$/$SrRuO_3$ device since the $(Fe_{Ti^{4+}}^{3+})'$ acceptors suppress semiconducting character of the $BaTiO_3$ thin film and make the polarization-modulation of the band diagram negligible. The present work facilitates the design of high-performance resistive memory devices based on ferroelectric diodes with controllable charged defects. *Published by AIP Publishing.*
[http://dx.doi.org/10.1063/1.4993938]

As a promising candidate for next-generation non-volatile memory technology, ferroelectric-induced resistance switching has attracted considerable attention owing to the advantages of high-density data storage, fast write/read speed, and non-destructive readout.[1,2] In general, a ferroelectric resistive memory is composed of a ferroelectric thin film sandwiched between two metallic electrodes, i.e., the metal/ferroelectric/metal (MFM) structure. Ferroelectric tunnel junctions and ferroelectric diodes are two typical categories of the ferroelectric resistive memories, in which transport along the thickness direction of the MFM device can be modulated between low (ON) and high (OFF) resistance states by the polarization reversal. Non-volatile resistive memory in the ferroelectric tunnel junctions originates from the modulation on the overall potential barrier profile by polarization switching in an ultrathin ferroelectric layer that allows electron tunneling between the two electrodes.[3] The ferroelectric diodes utilize a thick ferroelectric layer as a memory medium, and the resistance switching can be understood by the electrostatic screening of spontaneous polarization *via* the migration of carriers and/or charged defects and the bending of the energy band.[4] The ferroelectric diode is first proposed by Blom *et al.* in 1994 when the authors designed a Au/$PbTiO_3$/$La_{0.5}Sr_{0.5}CoO_3$ heterostructure with a Schottky barrier at the Au/$PbTiO_3$ top interface and observed an ON/OFF current ratio of $\sim 10^2$ due to the modulation of the Schottky barrier by the accumulation/depletion of charged defects *via* the polarization reversal of the 200 nm-thick $PbTiO_3$ thin film.[5] Later, Jiang *et al.* and Wang *et al.* achieved a switchable diode effect in Pt/$BiFeO_3$/$SrRuO_3$ heterostructures as a result of the two-side-modulation of the Schottky barriers at the top and the bottom metal/ferroelectric interfaces, respectively.[6,7] Ferroelectric-driven resistance switching has also been observed in a number of MFM diodes based on $BaTiO_3$ (BTO),[8,9] $Bi_4Ti_3O_{12}$,[10] $Hf_{0.5}Zr_{0.5}O_2$,[11] and poly(vinylidene fluoride) thin films,[12] as well as ferroelectric/dielectric bilayers.[13,14] In addition, several groups have demonstrated high-density data storage, as high as ~100 Gbit/in.^{2}, of the ferroelectric diodes in $BiFeO_3$ nano-island arrays grown on $SrRuO_3$ (SRO) and Nb:$SrTiO_3$ (STO) electrodes prepared by using an anodic aluminum oxide nano-template.[15–17] On the other hand, magnetoelectric three-state resistance switching,[18,19] memristive properties,[20,21] and switchable photoelectric effect[22–24] have also been achieved. These results suggest wide application of the ferroelectric diodes in nanoelectronic devices.

Most recently, Li *et al.* have pointed out in Au/BTO/$LaSrMnO_3$ devices that the resistance switching with a remarkable ON/OFF ratio can be observed only when there exists an appropriate concentration of ionic defects, such as the oxygen vacancies, in the BTO films through carefully controlling oxygen pressure in pulsed laser deposition (PLD).[8] Similar results have also been observed in Bi-deficient $BiFeO_3$ thin films.[25] In this work, we report another way of achieving enhanced resistive memory in ferroelectric diodes by doping the BTO thin film with donors. It is observed that the ON/OFF ratio of Au/BTO/SRO devices can be improved by about two orders of magnitude, from ~30 up to ~2000, due to the substitution of Ti^{4+} with Nb^{5+} ions, whereas the resistive memory is suppressed when Fe^{3+} ions are doped into the BTO thin film. The substitution-dependent resistance switching behaviors are discussed in terms of the modulation of band diagrams with polarization reversal and the transport analysis for the ON and OFF states at various temperatures.

Epitaxial BTO, 5 mol. % Nb-doped BTO (Nb:BTO), and 5 mol. % Fe-doped BTO (Fe:BTO) thin films, as well as SRO bottom electrodes were deposited on single-crystalline (001) $SrTiO_3$ (STO) substrates by PLD using a KrF excimer laser (Coherent COMPexPro 201). The STO substrates were etched by a NH_4F buffered-HF solution and annealed at

a)Author to whom correspondence should be addressed: zwen@qdu.edu.cn

950 °C for 1 h in flowing O_2 to form a TiO_2-terminated step-terrace surface. The SRO electrodes were deposited with a laser energy density of 3.5 J/cm^2 at a repetition rate of 4 Hz, keeping the substrate temperature at 650 °C and the O_2 pressure at 0.05 mbar. The BTO, Nb:BTO, and Fe:BTO layers were deposited with a laser energy density of 2.5 J/cm^2 and a repetition rate of 2 Hz at 700 °C and 0.05 mbar O_2 pressure. Au top electrodes of ~75 μm in diameter and ~50 nm in thickness were sputter-deposited on the heterostructures through a shadow mask to form diode devices. X-ray reflectivity (XRR) and X-ray diffraction (XRD) were performed on a Rigaku SmartLab X-ray diffractometer with Cu K_α radiation. Ferroelectric properties were measured by means of piezoresponse force microscopy (PFM) using an Asylum Research Cypher scanning probe microscope in the DART (dual a.c. resonance tracking) mode[26] and polarization-voltage (*P*-*V*) hysteresis loops on a Radiant Multiferroic ferroelectric tester at room temperature. Resistance switching properties of the ferroelectric diodes were recorded by using a Keithley 2400 SourceMeter on a LakeShore cryogenic probe station with voltage applied on the Au top electrode while the SRO electrode was always grounded through a Ag ohmic contact.

The thicknesses of BTO, Nb:BTO, Fe:BTO, and SRO thin films are controlled by accounting the laser pulse number and measured by XRR. Figure 1(a) shows the XRR pattern of a BTO(1500 laser pulses)/SRO(3000 laser pulses)/STO heterostructure, as an example. The clear intensity oscillations suggest smoothing interface and surface of the heterostructure. The thicknesses can be determined by fitting the XRR curve, which are ~30 and ~23 nm for the SRO and BTO layers, respectively. The BTO thickness as a function of laser pulse number is plotted in the inset. By extrapolation, the BTO layer (8000 laser pulses) adopted in the present work can be estimated, which is about 120 nm in thickness. Figure 1(b) shows XRD patterns of the BTO/SRO/STO, Nb:BTO/SRO/STO, and Fe:BTO/SRO/STO heterostructures, respectively. As shown, only (00 *l*) Bragg diffractions are observed, indicating epitaxial growth of the ferroelectric layers and the SRO electrodes on the STO (001) substrates.

As shown in Fig. 2(a), the Nb:BTO/SRO/STO heterostructure exhibits a smoothing surface with a root-mean-square roughness of ~0.8 nm. Similar atomic force microscopy (AFM) topography is also observed in BTO/SRO/STO and Fe:BTO/SRO/STO heterostructures. Saturated *P*-*V* hysteresis loops cannot be observed in the BTO and Nb:BTO thin films since the existence of oxygen vacancies $(V_{O^{2-}})^{\cdot\cdot}$ and $(Nb^{5+}_{Ti^{4+}})^{\cdot}$ donors, which increase the electron density in the films and make them n-type semiconductors.[8,27] PFM is hence adopted to measure room-temperature ferroelectric properties of the thin films. As shown in Fig. 2(b), typical PFM hysteresis loops are observed on the top electrode of the Au/Nb:BTO/SRO heterostructure, in which the coercive voltages are +4.0 and −2.8 V, respectively, as indicated by the minima of the amplitude loop. Au/BTO/SRO exhibits similar ferroelectric properties. For Au/Fe:BTO/SRO, a well-saturated *P*-*V* hysteresis loop is observed as the insulting properties of the Fe:BTO thin film are improved by incorporating $(Fe^{3+}_{Ti^{4+}})'$ acceptors that decrease the density of electrons, as shown in Fig. 2(c). The remnant polarization of

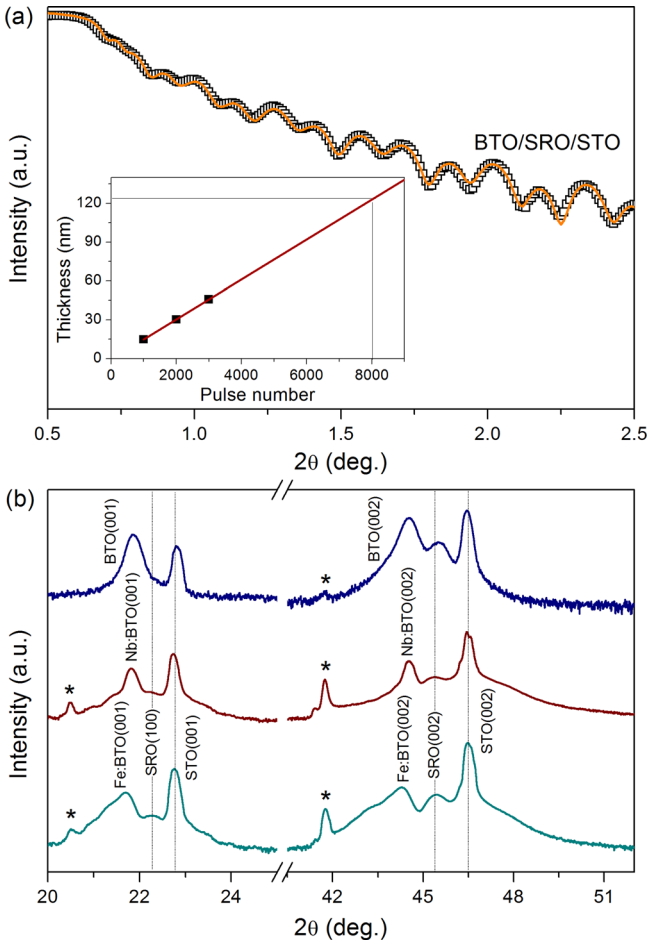

FIG. 1. (a) XRR pattern of a BTO/SRO/STO heterostructure, where the inset shows the BTO thickness as a function of laser pulse number. (b) XRD patterns of BTO/SRO/STO, Nb:BTO/SRO/STO, and Fe:BTO/SRO/STO heterostructures, respectively, where the * symbols denote Cu K_β lines from the Bragg diffraction of the STO single-crystalline substrates.

Fe:BTO is ~20 μC/cm^2, in good agreement with that reported previously in BTO thin films.[8,28]

Resistance switching of the Au/BTO/SRO, Au/Nb:BTO/SRO, and Au/Fe:BTO/SRO devices is measured by voltage sequence following $0 \rightarrow +V \rightarrow 0 \rightarrow -V \rightarrow 0$ applied on the Au top electrodes. As shown in Fig. 3, typical hysteretic current density-voltage (*J*-*V*) loops with rectifying characteristics are observed in the BTO and Nb:BTO ferroelectric diodes, indicating non-volatile resistive memory. The devices are switched from the high resistance OFF state to the low resistance ON state by applying +9.0 V and switched back to the OFF state by −9.0 V, as indicated by the arrows in Fig. 3. The resistance switching characteristics are also studied as a function of top electrode area, as shown in supplementary material Fig. S1. Both the ON and OFF states exhibit a monotonic increase in resistance with decreasing electrode area, suggesting that the resistance change takes place over the entire area of the interface, rather than a local phenomenon such as the formation/rupture of conductive filaments.[29] The voltage amplitude for resistance switching shown in Fig. 3 is consistent with that for polarization reversal in PFM hysteresis loops [Fig. 2(b)]. The ON/OFF ratio read at 2.0 V is ~30 in the Au/BTO/SRO device, which is comparable with that reported previously in BTO-based

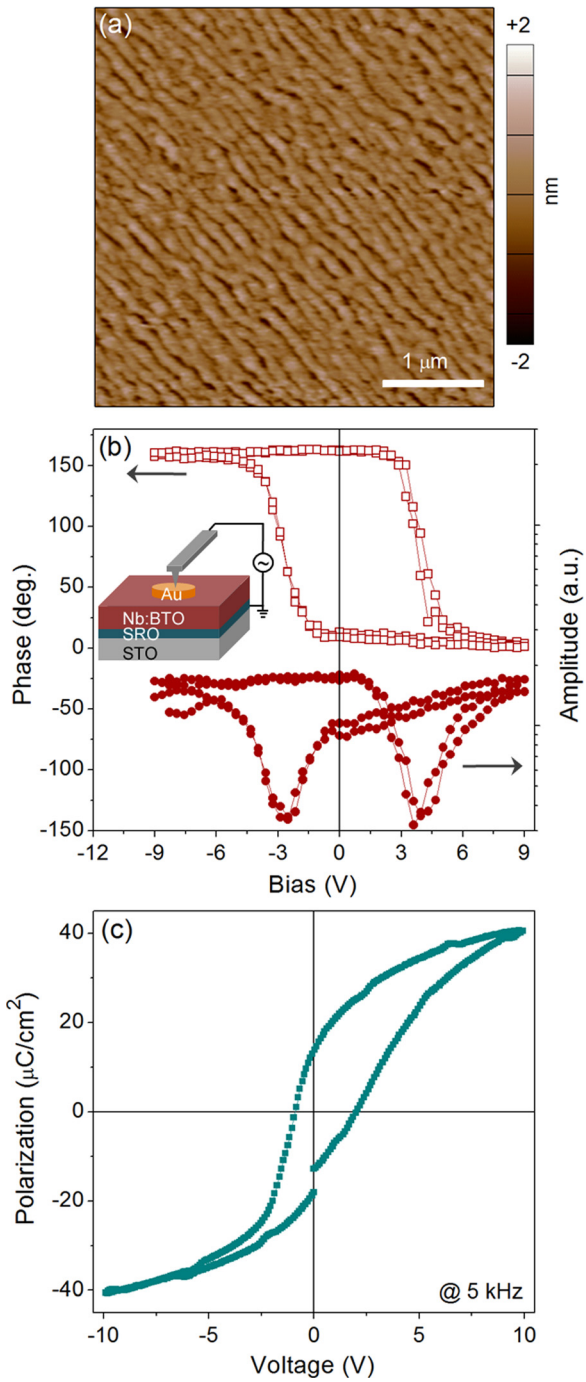

FIG. 2. (a) AFM topography of the Nb:BTO/SRO/STO heterostructure and (b) PFM phase and amplitude hysteresis loops of the Au/Nb:BTO/SRO, where the inset depicts the device structure and the PFM measurement. (c) *P-V* hysteresis loop of the Au/Fe:BTO/SRO device.

ferroelectric diodes with the same resistance switching polarity in response to the polarization switching.[8,9] By doping $(Nb^{5+}_{Ti^{4+}})^{\cdot}$ donors, the ON/OFF ratio can be significantly improved, which reaches to ~2000 in the Au/Nb:BTO/SRO ferroelectric diode, about two orders of magnitude higher than that of the Au/BTO/SRO, as shown in the bottom-left inset. In addition, the Nb:BTO device exhibits reproducibly bipolar resistance switching with an ON/OFF ratio of $\sim 10^3$ maintained after 500 write/erase cycles of ±8.0 V (the top-right inset). However, the resistance switching is suppressed in the Au/Fe:BTO/SRO device and there is almost no hysteretic

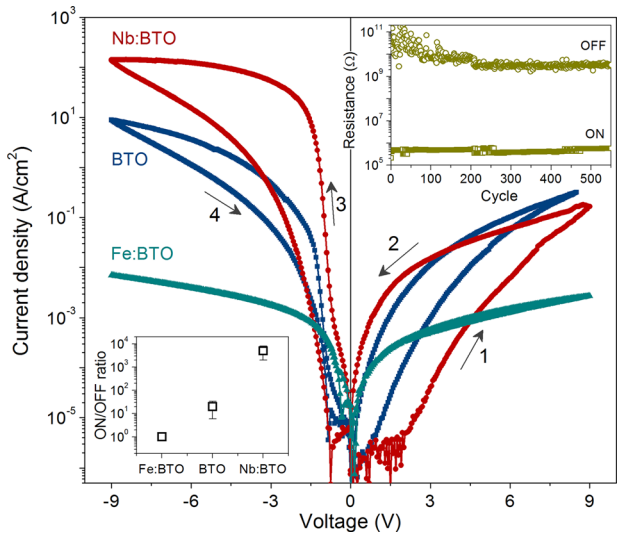

FIG. 3. Hysteretic *J-V* measurements of the Au/BTO/SRO, Au/Nb:BTO/SRO, and Au/Fe:BTO/SRO devices at room temperature, where the top-right inset shows bipolar resistance switching of the Au/Nb:BTO/SRO and the bottom-left inset plots ON/OFF ratios of these devices. Error bar in the bottom-left inset is average of five devices.

character observed in the *J-V* measurement, even though the Fe:BTO exhibits a well-saturated ferroelectric loop.

As reported previously in MFM ferroelectric diodes, the resistive memory is always associated with the switchable two-side diode effect due to the modulation of the Schottky barriers at the top and bottom metal/ferroelectric interfaces, respectively.[6,7,10,12] However, it is clear in Fig. 3 that the Au/BTO/SRO and Au/Nb:BTO/SRO devices exhibit one-side diode behaviors with reverse rectifying feature observed in both the ON and OFF states. Similar phenomena have also been observed in Pt/$BiFeO_3$/SRO devices and ascribed to the accumulation of $(V_{O^{2-}})^{\cdot\cdot}$ at the top interface.[30] Band diagrams of the Au/BTO/SRO diode are schematically demonstrated in Fig. 4(a), where the BTO is assumed as an n-type semiconductor since the existence of $(V_{O^{2-}})^{\cdot\cdot}$ that results in high density of electrons of the BTO and the rising of Fermi level (E_F) to approach the conduction-band minimum (~3.9 eV). Two Schottky barriers should be formed at the Au/BTO and BTO/SRO interfaces, respectively, if only taking into account the energy difference between the E_F of BTO and the work function of Au (~5.1 eV) and SRO (~5.2 eV). However, with an $(V_{O^{2-}})^{\cdot\cdot}$-rich layer at the Au/BTO interface, electrons accumulate on the BTO surface to neutralize the positively charged $(V_{O^{2-}})^{\cdot\cdot}$, which in turn results in downward-bending of the conduction band and the reduction (or even annihilation) of the Schottky barrier. Therefore, there is only one Schottky barrier at the BTO/SRO interface that dominates the transport, as shown in the middle band diagram in Fig. 4(a), where the BTO is assumed nonpolarized for clarity.

When the BTO is polarized pointing to the SRO, the depolarization field, resulting from incomplete screening of the ferroelectric bound charges, ionizes the neutral oxygen vacancies and drives electrons to the BTO/SRO interface. The Schottky barrier is reduced due to the electron accumulation, and the Au/BTO/SRO diode is hence switched to the ON state. If the interface barrier is thin enough and low

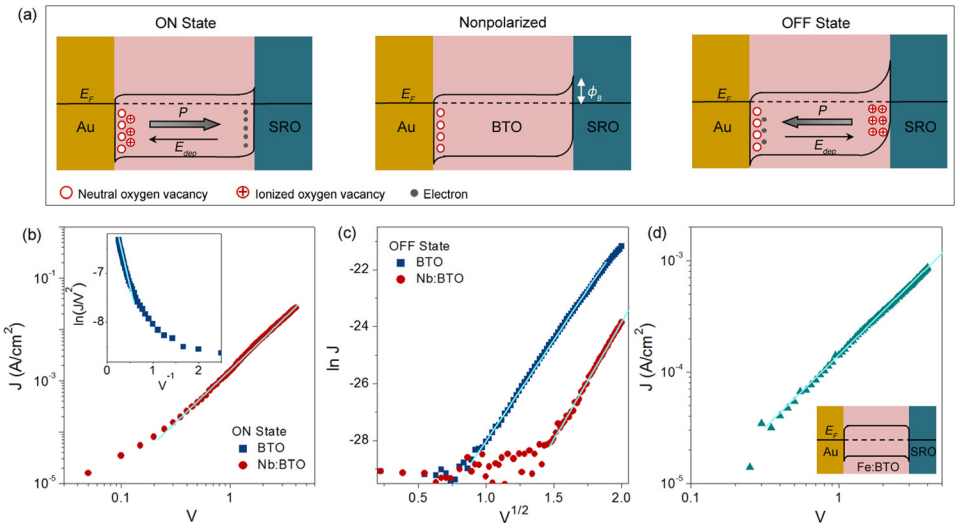

FIG. 4. (a) Band diagrams of the Au/BTO/SRO diode for the assumed non-polarized state, the ON state with polarization (P) pointing to the SRO electrode, and the OFF state with P pointing to the Au electrode. (b) The ON state J-V curves at positive bias for the Au/Nb:BTO/SRO in the log-log plot and for the Au/BTO/SRO in the $\ln(J/V^2)$-V^{-1} plot (the inset). (c) The OFF state J-V curves at positive bias of the two diodes in the $\ln J$-$V^{1/2}$ plot. (d) J-V curve at positive bias in the log-log plot of the Au/Fe:BTO/SRO, where the inset schematically shows the band diagram of this device.

enough, electron tunneling may take place, which obeys the Fowler-Nordheim tunneling mechanism,[31] as given by

$$J = B\left(\frac{V}{\delta}\right)^2 \exp\left(-\frac{C\delta\phi_B^{3/2}}{V}\right), \tag{1}$$

where B and C are the constants, ϕ_B is the potential barrier height, and δ is the barrier width. As shown in the inset in Fig. 4(b), the ON state J-V curve, extracted from the hysteretic J-V loop at positive bias from 0 to 4.0 V (Fig. 3), exhibits a linear relation between $\ln(J/V^2)$ and V^{-1}, suggesting that electron tunneling through a triangle-like interface barrier dominates the transport. The barrier, deduced from the fitting, is ~4.0 nm in width and ~0.6 eV in height. However, for the Au/Nb:BTO/SRO, the ON state J-V curve exhibits a slope of ~2.0 in the log-log plot [Fig. 4(b)], indicative of a bulk-limited space-charge-limit conduction,[32] which is expressed as

$$J = \frac{9}{8}\varepsilon_r\varepsilon_0\mu\frac{V^2}{d^3}, \tag{2}$$

where ε_r is the relative dielectric constant of the thin film, ε_0 the permittivity of free space, μ the charge carrier mobility, and d the thin film thickness. This suggests that the Schottky barrier is completely annihilated since there are more electrons accumulated at the Nb:BTO/SRO interface due to the existence of $(Nb_{Ti^{4+}}^{5+})^{\cdot}$ donors, compared to the Au/BTO/SRO. A large ON state current is thus observed in the Au/Nb:BTO/SRO, as shown in Fig. 3. Similar phenomena have also been reported in a SRO/n-BTO interface using first-principles calculation, in which the Schottky-type interface is even switched to an Ohmic contact by the polarization reversal.[33]

When the polarization is switched pointing to the Au electrode, the depolarization field drives positively charged $(V_{O^{2-}})^{\cdot\cdot}$ to the BTO/SRO interface, which increases the width of the space charge region and enhances the Schottky barrier, as shown in the right band diagram in Fig. 4(a). The BTO ferroelectric diode is thus switched to the OFF state. As shown in Fig. 4(c), $\ln J$ exhibits a linear increase with $V^{1/2}$, suggesting the dominant role of Schottky emission in the transport, which is given by[34]

$$J = A^*T^2\exp\left[-\frac{1}{k_BT}\left(\phi_B - \sqrt{\frac{q^3V}{4\pi\varepsilon_0\varepsilon_{opt}d}}\right)\right], \tag{3}$$

where A^* is the effective Richardson's constant, T the temperature (K), k_B the Boltzmann's constant, q the unit of electronic charge, and ε_{opt} the optical-frequency relative dielectric constant of the thin film. By fitting $\ln J$-$V^{1/2}$ to Eq. (3), ϕ_B can be determined from the intercept, which is 0.85 eV at the BTO/SRO interface, reasonable for the energy difference between the electron affinity of BTO and the work function of SRO. In the Au/Nb:BTO/SRO diode, the ϕ_B increases to 1.0 eV since there are not only the $(V_{O^{2-}})^{\cdot\cdot}$ but also the ionized donors of $(Nb_{Ti^{4+}}^{5+})^{\cdot}$ contributing to the space charge region at the Nb:BTO/SRO interface. The enhanced Schottky barrier results in the increased onset threshold for thermal emission and the suppressed OFF state current observed in the Au/Nb:BTO/SRO device, as shown in Figs. 3 and 4(c).

According to the above analysis, one can find that the significantly increased ON/OFF ratio achieved in the Au/Nb:BTO/SRO diode is a result of the enhanced ferroelectric-modulation on the interface potential barrier associated with the $(Nb_{Ti^{4+}}^{5+})^{\cdot}$ donors, which gives rise to an efficient control of transport between a bulk-limited current in the ON state and an interface-limited Schottky emission in the OFF state. In contrast, when $(Fe_{Ti^{4+}}^{3+})'$ acceptors are doped into the BTO layer, the concentration of electrons is suppressed and the Fe:BTO behaves as an insulator. The Au/Fe:BTO/SRO device exhibits a bulk-limited Ohmic conduction, as indicative of the slope close to unity in the $\log J$-$\log V$ plot [Fig. 4(d)], and almost no resistance switching character is observed since the polarization-modulation on the band diagram may be negligible with suppressed charged defects [the inset in Fig. 4(d)]. Figure 5 shows J-V loops of the Au/Nb:BTO/SRO diode recorded at various temperatures. It is clear that the resistive memory degrades with decreasing temperature, accompanied by the decrease in ϕ_B, as shown in the bottom-left inset. At 80 K, the resistance switching is quenched and the ϕ_B decreases to 0.25 eV. These phenomena may be ascribed to the decrease in thermally assisted ionization of neutral $(V_{O^{2-}})^{\cdot\cdot}$ and $(Nb_{Ti^{4+}}^{5+})^{\cdot}$ at low temperature.[35]

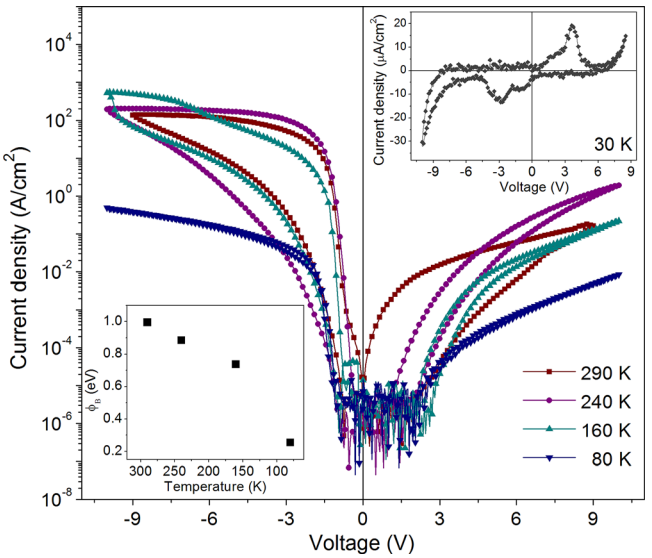

FIG. 5. *J-V* hysteretic loops of the Au/Nb:BTO/SRO ferroelectric diode recorded at various temperatures. The top-right inset shows the *J-V* measurement at 30 K and the bottom-left inset shows the OFF state ϕ_B as a function of temperature.

When temperature further decreases to 30 K, the thermally activate transport is also substantially suppressed and the transient current peaks from the polarization reversal of Nb:BTO are observed (the top-right inset).[35]

In summary, a large ON/OFF ratio of ~2000, about two orders higher than that of the Au/BTO/SRO, has been achieved in the Au/Nb:BTO/SRO ferroelectric diode at room temperature due to the doping of $(Nb^{5+}_{Ti^{4+}})^{\cdot}$ donors. The enhanced resistive memory performance is from efficient control of transport between a bulk-limited current in the ON state and an interface-limited Schottky emission in the OFF state, associated with the polarization reversal in the Nb:BTO thin film. However, the resistance switching is suppressed in the Au/Fe:BTO/SRO device and degrades with decreasing temperature. These results suggest the important function of the semiconducting ferroelectric layer with charged defects in resistance switching and facilitate the design of high-performance resistive memory devices based on ferroelectric diodes.

See supplementary material for the size-dependent resistance switching of the Au/BTO/SRO ferroelectric diode.

This work was jointly sponsored by the National Natural Science Foundation of China (Grant Nos. 11574169, 51472131, and 11504193), the Hong Kong Scholars Program (XJ2015024), and an innovation project of Qingdao (17-1-1-71-jch).

[1]C. Lu, W. Hu, Y. Tian, and T. Wu, Appl. Phys. Rev. **2**, 021304 (2015).
[2]S. Hong, *Emerging Non-Volatile Memories* (Spring, 2014), Chap. 5.
[3]V. Garcia and M. Bibes, Nat. Commun. **5**, 4289 (2014).
[4]S. Hong, S. M. Nakhmanson, and D. D. Fong, Rep. Prog. Phys. **79**, 076501 (2016).
[5]P. W. M. Blom, R. M. Wolf, J. F. M. Cillessen, and M. P. C. M. Krijn, Phys. Rev. Lett. **73**, 2107 (1994).
[6]A. Q. Jiang, C. Wang, K. J. Jin, X. B. Liu, J. F. Scott, C. S. Hwang, T. A. Tang, H. B. Lu, and G. Z. Yang, Adv. Mater. **23**, 1277 (2011).
[7]C. Wang, K. J. Jin, Z. T. Xu, L. Wang, C. Ge, H. B. Lu, H. Z. Guo, M. He, and G. Z. Yang, Appl. Phys. Lett. **98**, 192901 (2011).
[8]M. Li, J. Zhou, X. Jing, M. Zeng, S. Wu, J. Gao, Z. Zhang, X. Gao, X. Lu, J. M. Liu, and M. Alexe, Adv. Electron. Mater. **1**, 1500069 (2015).
[9]Y. A. Park, K. D. Sung, C. J. Won, J. H. Jung, and N. Hur, J. Appl. Phys. **114**, 094101 (2013).
[10]H. J. Song, J. B. Wang, X. L. Zhong, J. J. Cheng, L. H. Jia, F. Wang, and B. Li, Appl. Phys. Lett. **103**, 262901 (2013).
[11]Z. Fan, J. Xiao, J. Wang, L. Zhang, J. Deng, Z. Liu, Z. Dong, J. Wang, and J. Chen, Appl. Phys. Lett. **108**, 232905 (2016).
[12]B. B. Tian, Y. Liu, L. F. Chen, J. L. Wang, S. Sun, H. Shen, J. L. Sun, G. L. Yuan, S. Fusil, V. Garcia, B. Dkhil, X. J. Meng, and J. H. Chu, Sci. Rep. **5**, 18297 (2015).
[13]A. Tsurumaki-Fukuchi, H. Yamada, and A. Sawa, Appl. Phys. Lett. **103**, 152903 (2013).
[14]A. Tsurumaki-Fukuchi, H. Yamada, and A. Sawa, Appl. Phys. Lett. **104**, 092903 (2014).
[15]S. Hong, T. Choi, J. H. Jeon, Y. Kim, H. Lee, H. Y. Joo, I. Hwang, J. S. Kim, S. O. Kang, S. V. Kalinin, and B. H. Park, Adv. Mater. **25**, 2339 (2013).
[16]Z. Lu, Z. Fan, P. Li, H. Fan, G. Tian, X. Song, Z. Li, L. Zhao, K. Huang, F. Zhang, Z. Zhang, M. Zeng, X. Gao, J. Feng, J. Wan, and J. Liu, ACS Appl. Mater. Interfaces **8**, 23963 (2016).
[17]J. H. Jeon, H. Y. Joo, Y. M. Kim, D. H. Lee, J. S. Kim, Y. S. Kim, T. Choi, and B. H. Park, Sci. Rep. **6**, 23299 (2016).
[18]L. Feng, S. Yang, Y. Lin, D. Zhang, W. Huang, W. Zhao, Y. Yin, S. Dong, and X. Li, ACS Appl. Mater. Interfaces **7**, 26036 (2015).
[19]Y. P. Yao, Y. K. Liu, S. N. Dong, Y. W. Yin, S. W. Yang, and X. G. Li, Appl. Phys. Lett. **100**, 193504 (2012).
[20]Z. Hu, Q. Li, M. Li, Q. Wang, Y. Zhu, X. Liu, X. Zhao, Y. Liu, and S. Dong, Appl. Phys. Lett. **102**, 102901 (2013).
[21]X. Chen, C. H. Jia, Y. H. Chen, G. Yang, and W. F. Zhang, J. Phys. D: Appl. Phys. **47**, 365102 (2014).
[22]T. Choi, S. Lee, Y. J. Choi, V. Kiryukhin, and S. W. Cheong, Science **324**, 63 (2009).
[23]L. Wang, K. J. Jin, C. Ge, C. Wang, H. Z. Guo, H. B. Lu, and G. Z. Yang, Appl. Phys. Lett. **102**, 252907 (2013).
[24]R. Agarwal, Y. Sharma, and R. S. Katiyar, Appl. Phys. Lett. **107**, 162904 (2015).
[25]A. Tsurumaki-Fukuchi, H. Yamada, and A. Sawa, Adv. Funct. Mater. **22**, 1040 (2012).
[26]S. Jesse, A. P. Baddorf, and S. V. Kalinin, Appl. Phys. Lett. **88**, 062908 (2006).
[27]T. Kolodiazhnyi and S. C. Wimbush, Phys. Rev. Lett. **96**, 246404 (2006).
[28]F. Zhang, Y. B. Lin, H. Wu, Q. Miao, J. J. Gong, J. P. Chen, S. J. Wu, M. Zeng, X. S. Gao, and J. M. Liu, Chin. Phys. B **23**, 027702 (2014).
[29]A. Sawa, Mater. Today **11**, 28 (2008).
[30]D. Lee, S. H. Baek, T. H. Kim, J. G. Yoon, C. M. Folkman, C. B. Eom, and T. W. Noh, Phys. Rev. B **84**, 125305 (2011).
[31]R. H. Fowler and L. Nordheim, Proc. R. Soc. London, Ser. A **119**, 173 (1928).
[32]A. A. Grinberg, S. Luryi, M. R. Pinto, and N. L. Schryer, IEEE Trans. Electron Devices **36**, 1162 (1989).
[33]X. Liu, Y. Wang, J. D. Burton, and E. Y. Tsymbal, Phys. Rev. B **88**, 165139 (2013).
[34]S. M. Sze, *Physics of Semiconductor Devices*, 3rd ed. (Wiley-Interscience, Hoboken, 2007).
[35]Y. Lei, H. Zeng, W. Luo, Y. Shuai, X. Wei, N. Du, D. Burger, H. Skorupa, J. Liu, O. G. Schmidt, W. Zhang, and H. Schmidt, J. Mater. Sci.: Mater. Electron **27**, 7927 (2016).